An electron paramagnetic resonance study of Fe^{3+} centres in Tl_2MgF_4 and Tl_2ZnF_4 crystals

2006 J. Phys.: Condens. Matter 18 3053

(http://iopscience.iop.org/0953-8984/18/11/011)

INSTITUTE OF PHYSICS PUBLISHING JOURNAL OF PHYSICS: CONDENSED MATTER

J. Phys.: Condens. Matter **18** (2006) 3053–3067 doi:10.1088/0953-8984/18/11/011

An electron paramagnetic resonance study of Fe^{3+} centres in Tl_2MgF_4 and Tl_2ZnF_4 crystals

M Arakawa[1], A Okamoto[1], H Ebisu[2] and H Takeuchi[3]

[1] Department of Materials Science and Engineering, Nagoya Institute of Technology, Nagoya 466-8555, Japan
[2] Department of Electrical and Electronics Engineering, Nagoya Institute of Technology, Nagoya 466-8555, Japan
[3] Department of Advanced Science and Technology, Toyota Technological Institute, Nagoya, 468-8511, Japan

Received 6 January 2006
Published 1 March 2006
Online at stacks.iop.org/JPhysCM/18/3053

Abstract

EPR measurements have been made on as-grown single crystals of Tl_2MgF_4 and Tl_2ZnF_4 doped only with Fe and co-doped with Fe and Li using an X-band spectrometer. Signals from the charge-uncompensated Fe^{3+} centre with tetragonal symmetry (centre I) were observed for both crystals. Signals from an Fe^{3+} centre with monoclinic symmetry (centre II) were also observed for Tl_2ZnF_4. On the basis of the spin-Hamiltonian separation analysis, centre II is ascribed to an Fe^{3+} ion substituting for a Zn^{2+} ion with a nearest Tl^+ vacancy. The centre with orthorhombic symmetry (centre IV) observed in some Fe, Li co-doped Tl_2ZnF_4 crystals is ascribed to an Fe^{3+} ion associated with a Li^+ ion at the nearest Zn^{2+} site. Anomalies were found in the fine structure parameters b_2^0 for centres I and the separated parameters $b_{2a(1)}$ for centres II and IV, which have about double the magnitude of the corresponding values in Rb_2ZnF_4.

1. Introduction

K_2NiF_4-like layered perovskite crystals with space group $I4/mmm$ are interesting because of their close relationship to $KNiF_3$-like cubic perovskite crystals. The layered perovskite fluorides have a two-dimensional network of fluorine octahedra in contrast with the three-dimensional network of the octahedra in the cubic perovskite fluorides. Magnetic impurity ions doped in the layered perovskite fluorides are expected to substitute for host cations and form the magnetic impurity centres. In some cases, the trivalent magnetic M^{3+} ions substituting for the host divalent cations are associated with charge compensators for local charge neutrality. For these low symmetry M^{3+} centres the relationships between the fine structure parameters b_2^m ($m = 0, 2$) and the local environment around the magnetic ions were deduced by separating the fine structure terms into two uniaxial terms along the c axis with the parameter $b_{2a(1)}$ and along the direction to the charge compensator with the parameter $b_{2a(2)}$ [1–6].

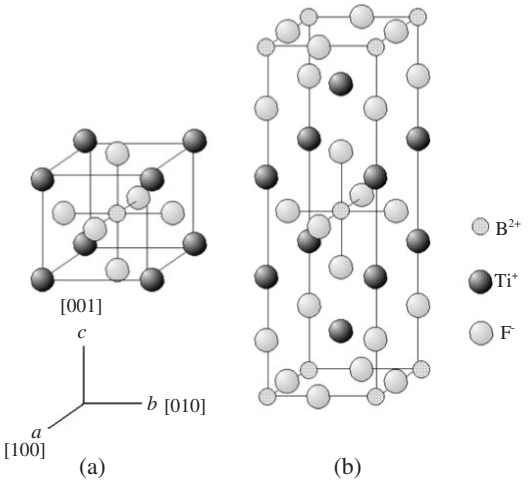

Figure 1. Unit cells of (a) a virtual cubic perovskite $TlBF_3$ crystal and (b) the layered perovskite Tl_2BF_4 (B = Mg, Zn) crystal.

The crystals of Tl_2MgF_4 and Tl_2ZnF_4 have the layered perovskite structure against the hexagonal-$BaTiO_3$ type structure of the $TlMgF_3$ and $TlZnF_3$ crystals [7]. Figure 1 shows the unit cell of Tl_2BF_4 (B = Mg or Zn). For the charge-uncompensated Cr^{3+} centres (Cr^{3+} centre I) in Tl_2ZnF_4 and Tl_2MgF_4, Arakawa *et al* [6, 8] reported the anomalies in the fine structure parameters: that the parameters b_2^0 have about double the magnitude of those in Rb_2ZnF_4 and K_2ZnF_4. The anomalies were also revealed in the separated parameters $b_{2a(1)}$ for the Cr^{3+}–V_{Tl} (Cr^{3+} centre II) and Cr^{3+}–Li^+ centres (Cr^{3+} centre IV) observed in these crystals. The information on the charge-compensated centres in the virtual cubic perovskite crystal $TlBF_3$ shown in figure 1(a) is obtained by the separated fine structure parameters $b_{2a(2)}$ of centres II and IV formed in the layered perovskite crystal Tl_2BF_4 shown in figure 1(b). It is interesting to examine whether any anomalies arise in Fe^{3+} centres formed in Tl_2BF_4.

Recently, Takeuchi *et al* [9] reported the results of EPR measurement for the trigonally symmetric Fe^{3+} centre in $CsMgCl_3$ crystal. The empirical rule for the relationship between the axial parameter b_2^0 and the trigonal distortion of the ligand octahedron has been proposed: that b_2^0 is positive for Fe^{3+} and negative for Cr^{3+} in the trigonally compressed ligand configuration and b_2^0 is negative for Fe^{3+} and positive for Cr^{3+} in the trigonally elongated ligand configuration. The magnitude of the ratio $b_2^0(Fe^{3+})/b_2^0(Cr^{3+})$ in $CsMgCl_3$ is about ten times larger than that for the K^+-vacancy-associated trigonal centre in $KZnF_3$. It may be valuable to examine whether the magnitudes of the ratio are extremely small in fluorides by the separated parameters $b_{2a(2)}$ for the Cr^{3+}–V_{Tl} and Fe^{3+}–V_{Tl} centres formed in the same layered perovskite crystal.

In this paper, we will report results of EPR measurements for the Fe^{3+} centres observed in Tl_2MgF_4 and Tl_2ZnF_4 single crystals. One kind of Fe^{3+} spectrum with tetragonal symmetry (Fe^{3+} centre I) was observed from the Tl_2MgF_4 crystal. For the Tl_2ZnF_4 crystal, Fe^{3+} spectra with tetragonal (Fe^{3+} centre I) and monoclinic (Fe^{3+} centre II) symmetries were observed. In the Tl_2ZnF_4 crystal co-doped with Fe and Li, a new Fe^{3+} spectrum with orthorhombic symmetry (Fe^{3+} centre IV) was observed together with that for centre I. The fine structure parameters for the centres II and IV will be analysed using the spin-Hamiltonian separation method in order to investigate the local environment around the Fe^{3+} ions. Magnitudes of

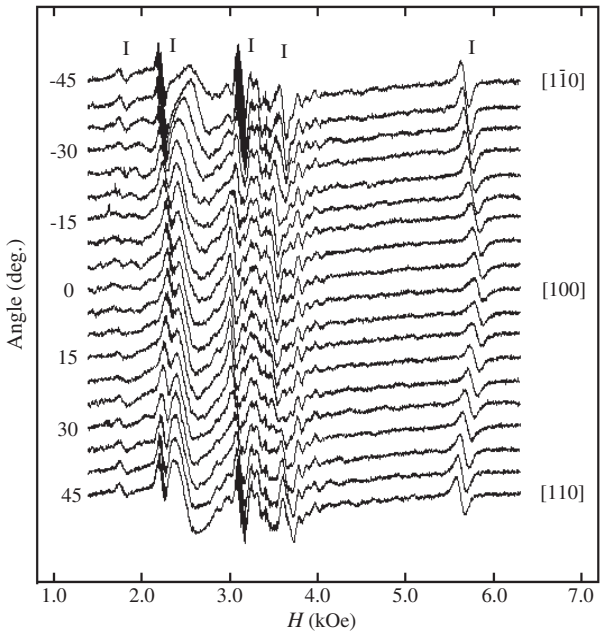

Figure 2. Angular variation of the EPR spectrum observed for the Fe, Li co-doped Tl_2MgF_4 crystal at room temperature with $\boldsymbol{H}$ in the c plane. The signals marked with I are those from an Fe^{3+} centre with tetragonal symmetry. Other unknown signals are also seen in the field range of 2.5–4.0 kOe.

b_2^0 for centres I and the separated parameters $b_{2a(1)}$ for centres II and IV will be examined in comparison with those for the corresponding Fe^{3+} centres in Rb_2ZnF_4. We will also examine the magnitude of the ratio $b_{2a(2)}(Fe^{3+})/b_{2a(2)}(Cr^{3+})$ for centre II in Tl_2ZnF_4.

2. Experimental procedures and results

Single crystals of Tl_2ZnF_4 were grown in graphite crucibles by the Bridgman technique. A trace of FeF_3 powder was added to the starting mixture of TlF and ZnF_2 powders. In some crystals, a small amount of LiF powder was added together with FeF_3. The crystals obtained are cleaved easily in the c plane. Single crystals of Tl_2MgF_4 were obtained in a similar manner from TlF and MgF_2 powders. The EPR measurements were made using a JES-FE1XG ESR spectrometer operating in the X band at the Advanced Instrument and Analysis Division in Nagoya Institute of Technology.

From the Tl_2MgF_4 crystals doped with only Fe, EPR spectra to be ascribed to any Fe^{3+} ions were not observed. In contrast, from the Tl_2MgF_4 crystals co-doped with Fe and Li, EPR signals of some Fe^{3+} ions are observed. Figure 2 shows the angular variation of the EPR spectra observed from the Fe, Li co-doped Tl_2MgF_4 crystal. The spectrum of the signals marked with I shows 90° periodicity with the external field $\boldsymbol{H}$ in the c plane. The fine structure of this spectrum shows a maximum splitting in the [001] field direction. These features indicate that the spectrum of the signals I has tetragonal symmetry about the crystalline c axis. So, we call it the tetragonal Fe^{3+} centre I in Tl_2MgF_4. Signals from other Fe^{3+} centres were not observed distinctly for the Tl_2MgF_4 crystals.

Figure 3 shows angular variation of the EPR spectra observed from an as-grown crystal of Tl_2ZnF_4 doped only with Fe. Two kinds of Fe^{3+} signals marked with I or II were observed. The

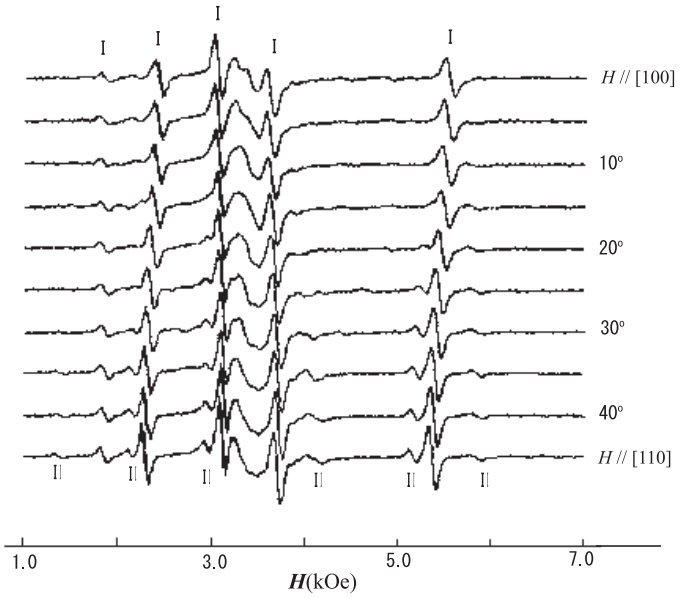

Figure 3. EPR spectra of the Fe^{3+} centres in the Fe-only-doped Tl_2ZnF_4 crystal observed at room temperature with $\boldsymbol{H}$ in the c plane. Signals for two kinds of Fe^{3+} spectra are distinguished by the marks I or II.

signals marked with II were observed with rather weak intensities in the field directions near $\boldsymbol{H} \parallel [110]$. In figure 4, observed resonant fields of signals I and II are plotted against external field direction in the c plane by open circles for signals I and by open squares for signals II. The spectrum of signals I shows a dependence of 90° periodicity similarly to the case of centre I in Tl_2MgF_4 shown in figure 2. Figure 5 shows angular variations of signals I and II with $\boldsymbol{H}$ declined from the [001] axis direction toward the [100] axis direction. The fine structure for the spectrum of signals I shows a maximum splitting in the [001] axis direction. The above features indicate that the spectrum of signals I observed in Tl_2ZnF_4 has tetragonal symmetry about the crystalline c axis. We call it the tetragonal Fe^{3+} centre I in Tl_2ZnF_4.

As seen from figures 4 and 5, angular variation of signals II splits into two branches in the field direction except for the [100] and [001] axes. In the c plane, each signal in the [100] direction splits into two branches, which have a peak or a trough in the [110] direction. In the (010) plane, each signal in the [001] field direction splits into two branches, one of which shows an extreme in the direction declined by about 5° from the c axis in contrast with the angular variation of centre I having the branches with the extremes in the [001] and [100] directions. It can be said from the above features that the spectrum of signals II has monoclinic symmetry with ⟨110⟩-symmetry planes. We call it the monoclinic Fe^{3+} centre II in Tl_2ZnF_4. The symmetry suggests the association of some charge compensator in the symmetry plane. The small tilt angle from the c axis for the maximum fine structure splitting shows that centre II is made by a small perturbation of centre I due to some charge compensator.

Figure 6(b) shows the recorder trace of the EPR signals observed at room temperature from the Fe, Li co-doped crystals of Tl_2ZnF_4 with $\boldsymbol{H} \parallel [100]$ axis. Weak EPR signals marked with IV were observed newly in the co-doped crystal together with the signals of centre I. Angular variation of signals IV against external field direction in the c plane is shown in figure 7, where the observed resonant fields are plotted by open circles. Each signal in the [110] direction

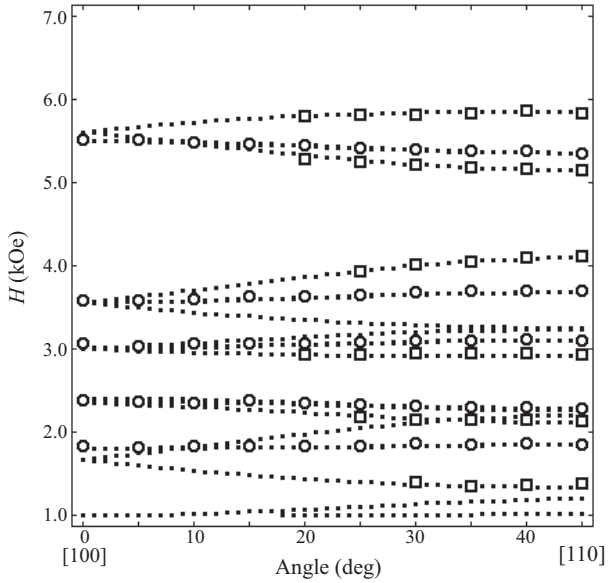

Figure 4. Angular variations of the signals I and II labelled in figure 3 with $\boldsymbol{H}$ in the c plane. Open circles and squares represent observed signals respectively due to the centres I and II in figure 3. Dotted curves denote the resonant fields calculated theoretically using the parameters listed in table 1.

splits into two branches, which have a peak or a trough in the [100] direction. The branches of signals IV in the (010) plane have peaks and troughs in the [001] and [100] directions. The fine structure of the spectrum shows a maximum splitting in the [001] direction. These features show that the spectrum of signals IV has orthorhombic symmetry. We call it the orthorhombic Fe^{3+} centre IV in Tl_2ZnF_4. The symmetry suggests the association of some charge compensator on the [100] or [010] axis.

The angular variation of the spectra for centres I in Tl_2MgF_4 and Tl_2ZnF_4 were described well by the following spin Hamiltonian having tetragonal symmetry with $S = \frac{5}{2}$:

$$\mathcal{H} = g_{\parallel}\beta S_z H_z + g_{\perp}\beta(S_x H_x + S_y H_y) + \tfrac{1}{3}b_2^0 O_2^0 + \tfrac{1}{60}[b_4^0 O_4^0 + b_4^4 O_4^4] \qquad (1)$$

where O_2^0, O_4^0 and O_4^4 are the Stevens operators defined in the text by Abragam and Bleaney [10]. The spin Hamiltonian is expressed in the coordinate system where the main principal z axis is chosen to be parallel to the crystalline c axis ([001] axis). The x axis is chosen to be parallel to the crystalline a axis ([100] axis).

The main principal axis direction for centre II in Tl_2ZnF_4 is declined from the c axis in the $(\bar{1}10)$ plane. By the small tilt angle of the main principal axis, centre II is regarded as the weakly perturbed centre for the tetragonal centre I. So, we try to describe the angular variation of the spectrum for centre II approximately using the following spin Hamiltonian having orthorhombic symmetry with $S = \frac{5}{2}$:

$$\mathcal{H} = g_z\beta S_z H_z + g_x\beta S_x H_x + g_y\beta S_y H_y + \tfrac{1}{3}[b_2^0 O_2^0 + b_2^2 O_2^2] + \tfrac{1}{60}[b_4^0 O_4^0 + b_4^2 O_4^2 + b_4^4 O_4^4], \qquad (2)$$

where the z axis is chosen to be parallel to the field direction showing the maximum fine structure splitting. The z axis direction is declined by an angle θ from the c axis in the $(\bar{1}10)$-symmetry plane, where the $\frac{1}{3}b_2^1 O_2^1$ term vanishes. The y axis is chosen to be parallel

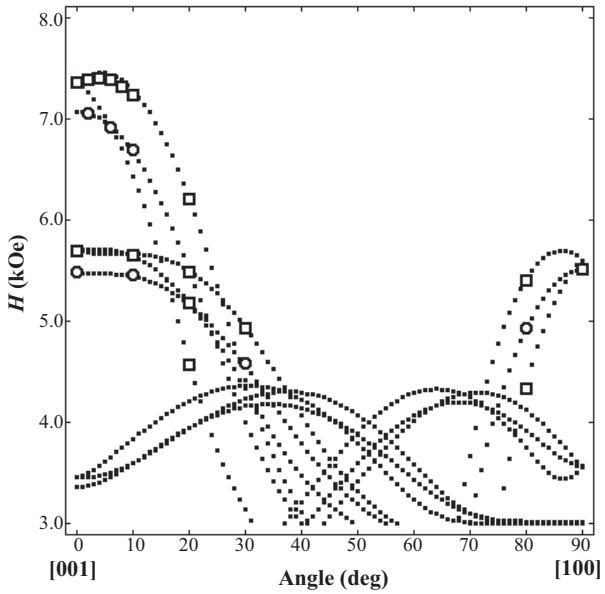

Figure 5. Angular variations of signals I and II observed from the Fe-doped Tl_2ZnF_4 with $\boldsymbol{H}$ in the (010) plane. The $\boldsymbol{H}$ is varied from the [001] direction (0°) toward the [100] direction (90°). Open circles and squares represent the observed resonant fields of signals I and II, respectively. Dotted curves denote the resonant fields calculated theoretically using the parameters listed in table 1.

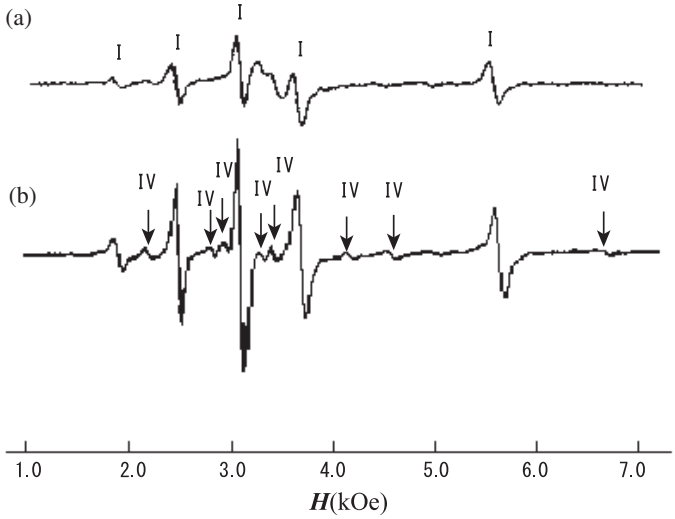

Figure 6. EPR spectra observed from Tl_2ZnF_4 at room temperature with $\boldsymbol{H} \parallel [100]$ for the crystals (a) doped only with Fe, and (b) co-doped with Fe and Li. The labels I denote the signals from the Fe^{3+} centre I. The labels IV denote the Fe^{3+} signals observed newly in the Fe, Li co-doped crystal.

to the $[\bar{1}10]$ direction. The x axis is in the $(\bar{1}10)$-symmetry plane. The observed spectrum was described well by the above spin Hamiltonian within the experimental errors.

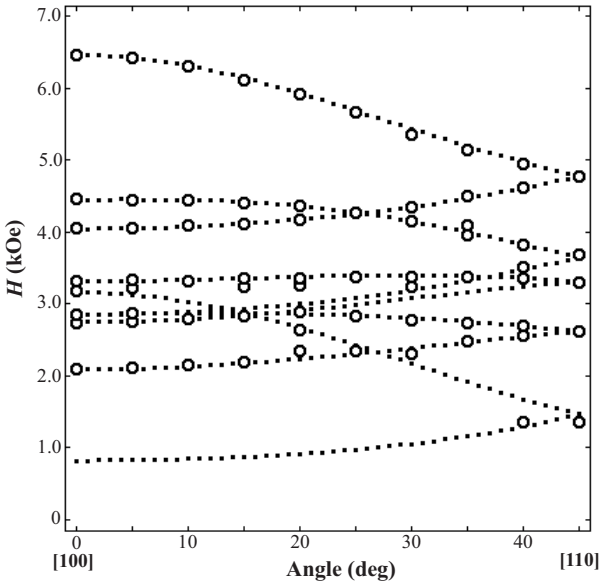

Figure 7. Angular variation of the signals IV labelled in figure 6 with $\boldsymbol{H}$ in the c plane. Open circles represent the resonant fields of the signals observed. Dotted curves denote the resonant fields calculated theoretically using the parameters listed in table 1.

The angular variation of the spectrum for centre IV in Tl_2ZnF_4 was described well by the following spin Hamiltonian having orthorhombic symmetry with $S = \frac{5}{2}$:

$$\mathcal{H} = g_z\beta S_z H_z + g_x\beta S_x H_x + g_y\beta S_y H_y + \tfrac{1}{3}[b_2^0 O_2^0 + b_2^2 O_2^2] + \tfrac{1}{60}[b_4^0 O_4^0 + b_4^2 O_4^2 + b_4^4 O_4^4]. \tag{3}$$

The spin Hamiltonian is expressed in the coordinate system where the z axis is parallel to the crystalline c axis and the x axis is parallel to the a axis.

The above spin Hamiltonians were fitted to the observed spectra by the direct matrix diagonalization method. The relative signs among the fine structure parameters b_n^m can be determined uniquely by the fitting. The absolute signs of the parameters b_n^m for centres I, II and IV and the angle θ for centre II were determined by the spin-Hamiltonian separation analysis to be mentioned in the following section. The spin-Hamiltonian parameters obtained for centres I, II and IV are listed in table 1. The dotted curves in figures 4, 5 and 7 are the theoretical resonant fields calculated using the spin-Hamiltonian parameters listed in table 1. Good agreement of the calculated values of the resonant fields with experimental ones is obtained.

3. Spin-Hamiltonian separation analysis

3.1. Centre I

The fine structure terms up to the fourth-rank Stevens operators for a tetragonal centre can be separated into uniaxial and cubic terms as follows:

$$\tfrac{1}{3}b_2^0 O_2^0(z) = \tfrac{1}{3}b_{2a} O_2^0(z), \tag{4a}$$

$$\tfrac{1}{60}\big[b_4^0 O_4^0(z) + b_4^4 O_4^4(x,y)\big] = \tfrac{1}{60}\Big[b_{4a} O_4^0(z) + b_{4c}\big(O_4^0(z) + 5O_4^4(x,y)\big)\Big]. \tag{4b}$$

Table 1. Spin-Hamiltonian parameters for the Fe^{3+} centres observed in Tl_2MgF_4 and Tl_2ZnF_4 at 300 K. The signs of the fine-structure parameters for centres II and IV and the sign of θ for centre II are determined as mentioned in section 3. Units are in 10^{-4} cm^{-1} for the fine structure parameters b_n^m.

Matrix Centre	Tl_2MgF_4 Centre I	Tl_2ZnF_4 Centre I	Tl_2ZnF_4 Centre II	Tl_2ZnF_4 Centre IV
g_x	2.0064(6)	2.0035(9)	1.998(6)	2.0004(6)
g_y	2.0064(6)	2.0035(9)	2.004(2)	2.0051(9)
g_z	1.9993(5)	2.0018(8)	2.0032(3)	1.9966(7)
b_2^0	−1016.6(4)	−900.4(6)	−991(2)	−781.4(4)
b_2^2	—	—	225(1)	610.0(7)
b_4^0	31.7(3)	33.6(4)	32(1)	33.5(3)
b_4^2	—	—	24(5)	25(2)
b_4^4	101(2)	107(2)	−89(19)	111(2)
θ (deg)	—	—	−5.1(2)	—

Table 2. Values of b_{2a}, b_{4a} and b_{4c} for the tetragonal Fe^{3+} centres (centre I) and values of $b_{2a(1)}$, $b_{4a(1)}$ and $b_{4c(1)}$ for the low symmetry Fe^{3+} centres (centres II, III and IV) in several layered perovskite fluorides. Units are in 10^{-4} cm^{-1}.

Crystal	Centre	b_{2a} $(=b_2^0)$	$b_{2a(1)}$	b_{4a}	$b_{4a(1)}$	b_{4c}	$b_{4c(1)}$
Tl_2MgF_4	I	−1016.6	—	11.5	—	20.5	—
Tl_2ZnF_4	I	−900.4	—	12.2	—	21.1	—
	II	—	−978	—	>0	—	>0
	IV	—	−984.7	—	16	—	13
Rb_2ZnF_4 [5]	I	−403.3	—	5.4	—	24.30	—
	II	—	−543.5	—	7.2	—	20.08
Rb_2CdF_4 [4]	I	−369.3	—	7.0	—	20.2	—
	III	—	−367.5	—	9.0	—	16.4

Equation (4*b*) is valid when the following conditions are satisfied:

$$b_{4a} = b_4^0 - \tfrac{1}{5}b_4^4, \qquad b_{4c} = \tfrac{1}{5}b_4^4. \tag{5}$$

The cubic parameter b_{4c} can be expected to have a positive sign similarly to b_4 for the cubic Fe^{3+} centre in $KZnF_3$ ($b_4 = +26.35 \times 10^{-4}$ cm^{-1}) [11]. This suggests a positive sign for the parameter b_4^4 as listed in table 1. We calculate the values of the separated fine structure parameters b_{4a} and b_{4c} for the Fe^{3+} centres I in Tl_2MgF_4 and Tl_2ZnF_4 from the experimental values of the raw parameters b_4^0 and b_4^4 using equation (5). Results are listed in table 2 together with b_{2a} $(=b_2^0)$. The values for the tetragonal Fe^{3+} centres (centre I) in Rb_2ZnF_4 and Rb_2CdF_4 are also listed for comparison.

In the spin-Hamiltonian separation analyses for a monoclinic or an orthorhombic Fe^{3+} centre, the second-rank fine structure terms are separated into two uniaxial terms with the parameters $b_{2a(1)}$ and $b_{2a(2)}$. The axial parameter $b_{2a(1)}$ is considered to represent the axiality along the c axis of the low symmetry Fe^{3+} centre, which corresponds to the axiality of the charge-uncompensated tetragonal Fe^{3+} centre. The other axial parameter $b_{2a(2)}$ is considered to represent the axiality of the perturbation due to some charge compensator. The parameters $b_{2a(1)}$ to be obtained later in sections 3.2 and 3.3 respectively for centres II and IV in Tl_2ZnF_4 are listed in table 2 together with the values of $b_{2a(1)}$ for centres II in Rb_2ZnF_4 and III in Rb_2CdF_4. Both the separated parameters $b_{2a(1)}$ for centres II and IV in Tl_2ZnF_4 have values close to the axial parameter b_{2a} for centre I in the same host crystal. This indicates that centre I

can be identified to be the charge-uncompensated Fe^{3+} centre, where the central Fe^{3+} ion is not associated with any charge compensators in its immediate neighbourhood.

For the Tl_2MgF_4 crystal co-doped with Fe and Li, the intense signals of the Fe^{3+} centre I are observed without signals from other Fe^{3+} centres. The spectrum has a tetragonal symmetry about the crystalline c axis. It may not be plausible to consider that the Fe^{3+} ion is preferentially associated with a Li^+ ion replaced for a Tl^+ ion on the c axis because Li^+ is a monovalent ion, the same as Tl^+. The parameter b_{2a} for Tl_2MgF_4 has a close value to that for Tl_2ZnF_4. So, centre I in the Fe, Li co-doped Tl_2MgF_4 is also identified to be the charge-uncompensated Fe^{3+} centre. In conclusion, both the centres I in Tl_2ZnF_4 and Tl_2MgF_4 are ascribable to the Fe^{3+} ions substituting for the divalent host cations without any charge compensators. It should be pointed out that the magnitudes of the parameters b_{2a} for centres I in the Tl compounds Tl_2MgF_4 and Tl_2ZnF_4 are about double the magnitude of that in Rb_2ZnF_4.

An anomaly of the fine structure parameters in Tl compounds is also found in the fourth-rank axial parameters b_{4a} for the centres I in Tl_2MgF_4 and Tl_2ZnF_4. The magnitudes of b_{4a} for these Tl compounds are about double the magnitude of that in Rb_2ZnF_4, as seen from table 2. On the other hand, the parameters b_{4c} for the Tl compounds have no anomalies. In the tetragonal centre, the axial parameter b_{4a} arises from the difference of the distance to the apical ligand on the c axis and the distance to the ligand in the c plane. The cubic parameter b_{4c} may be related to the distances to the projected points of ligands in the c plane. The above results obtained for the separated fourth-rank parameters b_{4a} and b_{4c} suggest that the anomaly is considered to happen because of some effects on the distortion of apical ligand F^- ions along the c axis by the existence of the nearest and the next-nearest Tl^+ ions in the crystals.

3.2. Centre II

For charge-compensated Fe^{3+} centres formed in layered perovskite fluorides, the relationship between the parameters b_2^m ($m = 0, 2$) and the local environments around the Fe^{3+} ions can be analysed using the spin-Hamiltonian separation method by separating the fine structure terms in the spin Hamiltonian into two uniaxial terms along the c axis and along the direction to the charge compensator.

Centre II with monoclinic symmetry was analysed approximately in the previous section using the spin Hamiltonian having orthorhombic symmetry as the weakly perturbed centre for tetragonal centre I by the association with some charge compensator in the $(\bar{1}10)$ plane. The fourth-rank fine structure terms in the spin Hamiltonian for centre II may be separated into the axial and cubic components corresponding to those for centre I and the additional axial component corresponding to the charge compensator as follows:

$$b_4^0 O_4^0(z) + b_4^2 O_4^2 + b_4^4 O_4^4(x, y) = b_{4a(1)} O_4^0(z') + b_{4c(1)}[O_4^0(z') - 5O_4^4(x', y')] + b_{4a(2)} O_4^0(z'') \tag{6}$$

where the z' axis is parallel to the crystalline c axis and the x' axis is chosen to be parallel to the [110] direction. It should be noticed that the coefficient of $O_4^4(x', y')$ in the cubic component term has negative sign (-5) since the x', y' axes are rotated by $\frac{\pi}{4}$ about the z axis from the x, y axes defined for centre I.

As mentioned in the previous section the principal z axis of the fine structure terms for centre II is declined only by 5.1° from the c axis in the $(\bar{1}10)$ plane. When the parameter $b_{4a(2)}$ is small, the parameter b_4^4 may be approximately estimated by $-5b_{4c(1)}$. As the sign of $b_{4c(1)}$ is considered to be positive, the same as the sign of b_{4c} for centre I, the absolute sign of b_4^4 for the centre II can be determined to be negative. Then, the absolute signs of b_n^m for centre II are determined by the selection of a negative sign of b_4^4 as listed in table 1.

Table 3. Value of $b_{2a(2)}$ for the Fe^{3+} centre II in Tl_2ZnF_4 together with that for the Fe^{3+} centre II in Rb_2ZnF_4. The value of b_2^0 for the Fe^{3+}–V_K centre in $KZnF_3$ is listed for comparison. Units are in 10^{-4} cm^{-1} for the fine structure parameters.

Crystal	Centre	b_2^0	$b_{2a(2)}$	Symmetry
Tl_2ZnF_4	Fe^{3+}–V_{Tl}	—	212	Monoclinic
Rb_2ZnF_4 [5]	Fe^{3+}–V_{Rb}	—	185.5	Monoclinic
$KZnF_3$ [13]	Fe^{3+}–V_K	103.4	—	Trigonal

In our previous work, the monoclinic Fe^{3+} centre in Rb_2ZnF_4 showed the maximum fine structure splitting in the field direction declined by about 7° from the c axis in the $(\bar{1}10)$ plane and was ascribed to an Fe^{3+} ion associated with a nearest Rb^+ vacancy by the spin-Hamiltonian separation analysis. So, in the present monoclinic Fe^{3+} centre II in Tl_2ZnF_4, the association of a vacancy at the nearest Tl^+ site in the $(\bar{1}10)$ plane is expected. We try to separate the second-rank fine structure terms for centre II into two uniaxial terms as follows:

$$b_2^0 O_2^0(z) + b_2^2 O_2^2(x, y) = b_{2a(1)} O_2^0(z') + b_{2a(2)} O_2^0(z''), \tag{7}$$

where the z'' axis is declined by 54.7° (=$\cos^{-1}(1/\sqrt{3})$) from the c axis toward the x axis in the $(\bar{1}10)$ plane. By the calculation using the transformation properties of the Stevens operators given by Rudowicz [12], we deduce that equation (7) holds if the following conditions are satisfied:

$$b_{2a(1)} = \frac{3\cos^2\theta - 1}{2} b_2^0 + \frac{\sin^2\theta}{2} b_2^2, \tag{8}$$

$$b_{2a(2)} = \frac{3\sin^2\theta}{2} b_2^0 + \frac{\cos^2\theta + 1}{2} b_2^2, \tag{9}$$

$$\sin 2\theta = \frac{2\sqrt{2} b_{2a(2)}}{3b_2^0 - b_2^2}. \tag{10}$$

In the separation with the z'' axis along the above-mentioned direction, the conditions (8)–(10) are approximate relations. Here, we calculate the separated axial parameters $b_{2a(1)}$ and $b_{2a(2)}$ by equations (8) and (9) using the experimental values of b_2^0, b_2^2 and θ in table 1. Then, equation (10) may be regarded as the criterion for the applicability of the separation. That is, the separation is good for the value of the ratio $R_2 = [2\sqrt{2}b_{2a(2)}]/[(3b_2^0 - b_2^2)\sin 2\theta]$ close to unity. In this case, we obtain a good value as $R_2 = 1.09$.

Obtained values of the separated parameters for the Fe^{3+} centre II in Tl_2ZnF_4 are tabulated in tables 2 and 3. The axial parameter $b_{2a(1)}$ has the value close to b_{2a} for centre I. This result shows that the negative sign of b_2^0 listed for centre II in table 1 is appropriate. It should be emphasized that the value of $b_{2a(2)}$ for the Fe^{3+} centre II in Tl_2ZnF_4 is close to that of the Fe^{3+} centre associated with the nearest Rb^+ vacancy in Rb_2ZnF_4 although the values of b_2^0 for both centres are rather different. The $b_{2a(2)}$ value has the same positive sign as that of b_{2a} for the Fe^{3+} centre associated with the nearest K^+ vacancy in the cubic perovskite fluoride $KZnF_3$. The above result is consistent with the expectation that centre II in Tl_2ZnF_4 is ascribed to an Fe^{3+} ion associated with the nearest Tl^+ vacancy.

It is considered that the excess positive charge on the Fe^{3+} ion is locally just compensated by the Tl^+ vacancy located at the direction declined by about 55° from the c axis in the $(\bar{1}10)$ plane. The sign of the angle θ is determined to be negative from equation (10). This indicates that the main principal axis of the centre is declined from the c axis toward the opposite direction to the vacancy. A schematic model of centre II is shown in figure 8. It is concluded

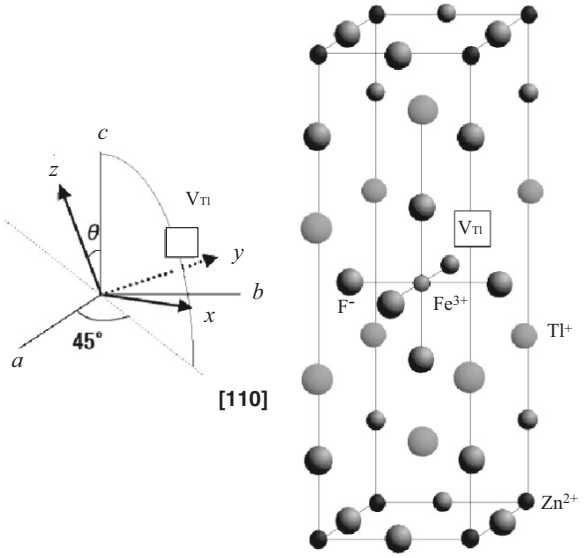

Figure 8. Relationship between the direction to the nearest Tl^+ vacancy and the principal axes of the fine structure terms for centre II in Tl_2ZnF_4.

that centre II is ascribed to an Fe^{3+} ion associated with the nearest Tl^+ vacancy in spite of the small tilt angle of the main principal z axis.

3.3. Centre IV

The spectrum of centre IV is observed only from the Fe, Li co-doped Tl_2ZnF_4 crystal. The angular variation of the resonant fields shows the orthorhombic symmetry with the main principal z axis along the crystalline c axis. From the above features, centre IV is considered to be an Fe^{3+} centre associated with a Li^+ ion as a charge compensator. The Fe^{3+} ion may substitute for a Zn^{2+} ion similarly to centre I, and the Li^+ ion may exist on the crystalline $\langle 100 \rangle$ axes in the c plane as a charge compensator for local neutrality.

We try to analyse centre IV by two types of spin-Hamiltonian separation for the second-rank fine structure terms to determine the position of the charge compensator. That is, the following separation types I and II are considered:

$$\text{(Type I):} \quad b_2^0 O_2^0(z) + b_2^2 O_2^2(x, y) = b_{2a(1)} O_2^0(z) + b_{2a(2)} O_2^0(x), \tag{11}$$

and

$$\text{(Type II):} \quad b_2^0 O_2^0(z) + b_2^2 O_2^2(x, y) = b_{2a(1)} O_2^0(z) + b_{2a(2)} O_2^0(y), \tag{12}$$

where the x, y and z axes are respectively parallel to the crystalline a, b and c axes. The Stevens operators are defined as

$$O_2^0(x) = 3S_x^2 - S(S+1), \quad O_2^0(y) = 3S_y^2 - S(S+1), \quad O_2^0(z) = 3S_z^2 - S(S+1),$$
$$O_2^2(x, y) = S_x^2 - S_y^2. \tag{13}$$

Equation (11) holds when the following conditions are satisfied:

$$\text{(Type I):} \quad b_{2a(1)} = b_2^0 + \tfrac{1}{3} b_2^2, \qquad b_{2a(2)} = \tfrac{2}{3} b_2^2. \tag{14}$$

Equation (12) holds when the following conditions are satisfied:

$$\text{(Type II):} \quad b_{2a(1)} = b_2^0 - \tfrac{1}{3} b_2^2, \qquad b_{2a(2)} = -\tfrac{2}{3} b_2^2. \tag{15}$$

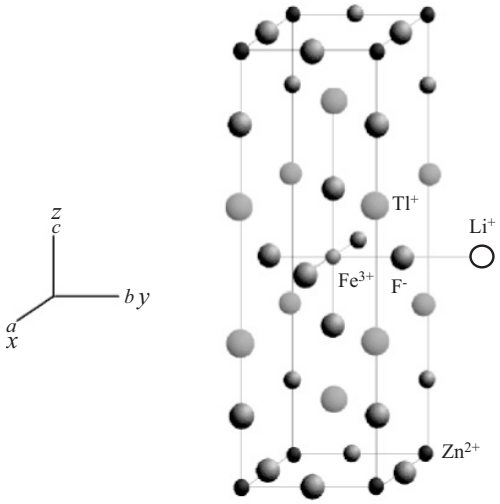

Figure 9. Schematic model and relationship between the principal axes of the fine structure terms for the Fe^{3+} centre IV in Tl_2ZnF_4.

Table 4. Values of $b_{2a(2)}$, $b_{4a(2)}$ and their ratio $b_{4a(2)}/b_{2a(2)}$ for the Fe^{3+} centre IV in Tl_2ZnF_4. Values for the Fe^{3+}–V_{Cd} centre in Rb_2CdF_4 and for the Fe^{3+}–Li^+ and the Fe^{3+}–V_{Cd} centres in perovskite fluorides are also listed for comparison. Units are in 10^{-4} cm^{-1} for the fine structure parameters.

Crystal	Centre	b_{2a}	$b_{2a(2)}$	b_{4a}	$b_{4a(2)}$	$b_{4a(2)}/b_{2a(2)}$
Tl_2ZnF_4	Fe^{3+}–Li^+	—	−406.7	—	10	−0.025
$RbCdF_3$ [14]	Fe^{3+}–Li^+	−603.6	—	10.0	—	−0.017
$CsCdF_3$ [14]	Fe^{3+}–Li^+	−800.9	—	11.7	—	−0.015
Rb_2CdF_4 [4]	Fe^{3+}–V_{Cd}	—	−304.5	—	6.6	−0.022
$RbCdF_3$ [14]	Fe^{3+}–V_{Cd}	−421.7	—	6.0	—	−0.014
$CsCdF_3$ [14]	Fe^{3+}–V_{Cd}	−547.7	—	6.5	—	−0.012

We can calculate the separated axial parameters $b_{2a(1)}$ and $b_{2a(2)}$ for each type of the separation by equations (14) or (15) from the experimental values of b_2^0 and b_2^2 in table 1. Calculated values are $b_{2a(1)} = -578.1 \times 10^{-4}$ cm^{-1} and $b_{2a(2)} = 406.7 \times 10^{-4}$ cm^{-1} for type I and $b_{2a(1)} = -984.7 \times 10^{-4}$ cm^{-1} and $b_{2a(2)} = -406.7 \times 10^{-4}$ cm^{-1} for type II. It is pointed out that the values of $b_{2a(2)}$ for both separations have the same magnitudes. In our previous works [14], the values of b_2^0 for the Fe^{3+}–Li^+ centres and the Fe^{3+}–V_{Cd} centres with tetragonal symmetries in perovskite fluorides were found to have negative signs. So, we choose the negative sign for the separated axial parameter $b_{2a(2)}$ on the assumption that the charge compensator is a Li^+ ion on the y axis (type II).

In tables 2 and 4, obtained values of the separated parameters $b_{2a(1)}$ and $b_{2a(2)}$ for the separation type II are listed together with the corresponding separated parameters for the orthorhombic Fe^{3+} centres III and IV reported previously for the cubic perovskite and layered perovskite fluorides. The separated parameter $b_{2a(1)}$ is close to b_2^0 for the Fe^{3+} centre I in Tl_2ZnF_4. This supports the separation type II, which corresponds to the Fe^{3+} ion substituting for a Zn^{2+} ion associated with a Li^+ ion at the nearest Zn^{2+} site on the y axis (b axis). A schematic model of centre IV is shown in figure 9.

Table 5. Values of b_2^0 for the charge-uncompensated Fe^{3+} and Cr^{3+} centres (centre I) in several layered perovskite fluorides. The ratios of b_2^0 for the Fe^{3+} centre to that for the corresponding Cr^{3+} centre in the same host crystals are given in the last column. Units are in 10^{-4} cm^{-1} for the fine structure parameters.

Crystal	a (Å)	c (Å)	c/a	b_2^0(Fe)	b_2^0(Cr)	b_2^0(Fe)/b_2^0(Cr)
Tl_2MgF_4	4.007	14.43 [7]	3.60	−1016.6	−1041.7 [8]	0.98
Tl_2ZnF_4	4.105	14.10 [7]	3.43	−900.4	−866.1 [6]	1.04
Rb_2ZnF_4	4.136	13.706 [15]	3.31	−403.3 [5]	−369.0 [2]	1.09

Next, we separate the fourth-rank fine structure terms for the Fe^{3+} centre IV into two uniaxial terms and a cubic term in the type II scheme as follows:

$$b_4^0O_4^0 + b_4^2O_4^2 + b_4^4O_4^4 = b_{4a(1)}O_4^0(z) + b_{4a(2)}O_4^0(y) + b_{4c(1)}\Big[O_4^0(z) + 5O_4^4(x, y)\Big]. \tag{16}$$

Equation (16) holds when the following conditions are satisfied:

$$b_{4a(1)} = b_4^0 + \tfrac{1}{5}b_4^2 - \tfrac{1}{5}b_4^4, \qquad b_{4a(2)} = \tfrac{2}{5}b_4^2, \tag{17}$$

$$b_{4c(1)} = -\tfrac{7}{20}b_4^2 + \tfrac{1}{5}b_4^4. \tag{18}$$

The absolute signs of b_n^m for centre IV can be determined by the selection of a positive sign for $b_{4c(1)}$. We calculate the separated axial parameters $b_{4a(1)}$, $b_{4a(2)}$ and the separated cubic parameter $b_{4c(1)}$ by equations (17) and (18) from the experimental values of b_4^0, b_4^2 and b_4^4 listed in table 1. Obtained values are tabulated in tables 2 and 4. The value of $b_{4a(2)}$ for the Fe^{3+} centre IV in Tl_2ZnF_4 is close to the parameters b_{4a} for the Fe^{3+}–Li^+ centres in $RbCdF_3$ and $CsCdF_3$. The situation is similar to the Fe^{3+}–V_{Cd} centre in Rb_2CdF_4 as seen from table 4, although the magnitude of $b_{4a(2)}$ is rather different for both cases. It is concluded from the above analysis together with the results for $b_{2a(2)}$ that the Fe^{3+} centre IV is associated with a Li^+ ion at the nearest Zn^{2+} site.

4. Discussion

We compare the values of b_2^0 for the charge-uncompensated Fe^{3+} centres (Fe^{3+} centre I) with those for the charge-uncompensated Cr^{3+} centres (Cr^{3+} centre I) in the same layered perovskite fluorides. In table 5, the values of b_2^0 for the Fe^{3+} centres I are denoted by b_2^0(Fe) and those for the Cr^{3+} centres I are denoted by b_2^0(Cr). The magnitudes of b_2^0(Fe) and b_2^0(Cr) for Tl_2ZnF_4 are close to the corresponding values for Tl_2MgF_4 within the Tl compounds, but about double the magnitudes of the corresponding values for Rb_2ZnF_4. As a result, the ratios b_2^0(Fe)/b_2^0(Cr) are close to unity for all the three compounds.

This shows that the anomalies of b_2^0 found for the centres I in the Tl compounds Tl_2MgF_4 and Tl_2ZnF_4 occur commonly for both the Fe^{3+} and Cr^{3+} centres. So, the Tl^+ ions in the crystals are considered to affect the local distortions of ligands around the Fe^{3+} and Cr^{3+} ions in rather different manner from the cases in the crystals having Rb^+ cation. In this respect, the lattice parameter c of Tl_2ZnF_4 is larger than that of Rb_2ZnF_4 although the ionic radius (1.47 Å) of Tl^+ is the same as that of Rb^+. The magnitudes of b_2^0 for both Fe^{3+} and Cr^{3+} in Tl_2MgF_4 are larger than those in Tl_2ZnF_4. In Tl_2MgF_4, a is smaller and c is larger than the corresponding values in Tl_2ZnF_4. This suggests that two ligand fluorines on the c axis deviate easily in Tl_2MgF_4 and Tl_2ZnF_4. The anomalously large magnitudes of b_2^0 for centres I in Tl compounds may be caused by large compression of ligand octahedra along the c axis.

Recently, Takeuchi *et al* [9] proposed an empirical rule for the relationship between the axial parameter b_2^0 and the trigonal distortion of the ligand octahedron: that the parameter b_2^0

Table 6. Values of $b_{2a(2)}$ derived for the Fe^{3+} and Cr^{3+} centres II (M^{3+}–V_A centre) and IV (M^{3+}–Li^+ centre) in layered perovskite fluorides and values of b_{2a} for the same kinds of centre with trigonal and tetragonal symmetries in the cubic perovskite fluorides. Units are in 10^{-4} cm^{-1} for the fine structure parameters.

Crystal	Centre	$b_{2a(2)}$(Fe)	$b_{2a(2)}$(Cr)	$b_{2a(2)}$(Fe)/$b_{2a(2)}$(Cr)	Symmetry
Tl_2ZnF_4	M^{3+}–V_{Tl}	211.2	−1375.1 [6]	−0.15	Monoclinic
$KZnF_3$	M^{3+}–V_K	103.4 [13]	−1613.0 [16]	−0.06	Trigonal
$CsMgCl_3$	M^{3+}	−796.7 [9]	1253.3 [17]	−0.64	Trigonal
Al_2O_3	M^{3+}	1679 [18]	−1920 [19]	−0.87	Trigonal
Tl_2ZnF_4	M^{3+}–Li^+	−406.7	−508.3 [8]	0.80	Orthorhombic
$RbCdF_3$	M^{3+}–Li^+	−603.6 [14]	−743.9 [20]	0.81	Tetragonal
$KZnF_3$	M^{3+}–Li^+	−759.0 [21]	−542.1 [20]	1.40	Tetragonal

for Fe^{3+} has different sign from that for Cr^{3+}. The magnitude of the ratio $b_2^0(Fe^{3+})/b_2^0(Cr^{3+})$ for the charge-uncompensated centres in $CsMgCl_3$ is about ten times larger than that for the K^+-vacancy associated trigonal centres in $KZnF_3$. This suggests that the magnitude of b_2^0 for the trigonal Fe^{3+} centre relative to the same type of Cr^{3+} centre in the same matrix is also extremely small in other fluoride matrices. The separated parameters $b_{2a(2)}$ for the monoclinic centres II in Tl_2ZnF_4 may be regarded as the axial parameters b_2^0 for the Tl^+-vacancy-associated trigonal centres formed in a virtual cubic $TlZnF_3$ crystal, although the real crystal of $TlZnF_3$ has the hexagonal-$BaTiO_3$ type structure. The ratio of the separated parameters $b_{2a(2)}(Fe)/b_{2a(2)}(Cr)$ for centre II in layered perovskite fluoride is compared in table 6. The ratio for centres II in Tl_2ZnF_4 has the same negative sign as that for the M^{3+}–V_K centre in $KZnF_3$. The magnitudes are smaller than those in $CsMgCl_3$ and Al_2O_3. In conclusion, there exists an empirical rule that the ratio of $b_2^0(Fe^{3+})/b_2^0(Cr^{3+})$ for trigonal distortion in fluorides is considerably smaller than those in chlorides and oxides.

The separated parameters $b_{2a(2)}$ for the centres IV in Tl_2ZnF_4 can be regarded as the axial parameters for the tetragonal M^{3+} centres (M = Fe, Cr) with a Li^+ at the nearest divalent cation site in a virtual cubic $TlZnF_3$ crystal. The ratios $b_{2a(2)}(Fe)/b_{2a(2)}(Cr)$ for centres IV are listed in table 6 together with those for the same kind of M^{3+}–Li^+ centres with tetragonal symmetry in the cubic perovskites $KZnF_3$ and $RbCdF_3$. The ratio is comparable with those for the M^{3+}–Li^+ centre in cubic perovskite fluorides. The result suggests that the local distortions around the Fe^{3+} ion occur similarly to the case of Cr^{3+} ion for centre IV.

5. Conclusion

Two kinds of EPR spectra from the Fe^{3+} centres have been observed from the Tl_2ZnF_4 crystals doped with Fe. One comprises the signals from the tetragonal Fe^{3+} centre (centre I) and the other comprises the signals from the monoclinic centre (centre II). The EPR spectrum for the orthorhombic Fe^{3+} centre (centre IV) has been observed only from the crystals co-doped with Fe and Li. For the low symmetry centres II and IV, the fine structure parameters are analysed by the spin-Hamiltonian separation method. The separated parameters $b_{2a(1)}$ for centres II and IV have values close to the parameter b_2^0 for centre I. The tetragonal centre I is identified to be the charge-uncompensated centre where an Fe^{3+} ion substitutes for a Zn^{2+} ion without any charge compensators in its immediate neighbourhood. The monoclinic centre II is ascribed to an Fe^{3+} ion associated with the nearest Tl^+ vacancy (the Fe^{3+}–V_{Tl} centre). The orthorhombic centre IV is ascribed to an Fe^{3+} ion associated with a Li^+ ion at the nearest Zn^{2+} site in the *c* plane (the Fe^{3+}–Li^+ centre). In Tl_2MgF_4 crystals only the signals from the charge-uncompensated Fe^{3+} centre (centre I) have been observed.

Anomalies are found in the axial parameters b_{2a} and b_{4a} for centres I in Tl_2ZnF_4 and Tl_2MgF_4 crystals and in the separated axial parameters $b_{2a(1)}$ for centres II and IV in Tl_2ZnF_4. These axial fine structure parameters have about double the magnitude of that for Rb_2ZnF_4. The cubic parameters b_{4c} for centres I showed no anomalies. The result suggests that the anomalies in the axial parameters may come from the effects of the nearby Tl^+ ions on the local distortion of apical ligand F^- ions along the c axis.

It is found from the separated parameter $b_{2a(2)}$ for the centre II in Tl_2ZnF_4 that its magnitude for the Fe^{3+} centre is extremely small relative to that for the corresponding Cr^{3+} centre in the same matrix. The result supports the empirical rule that the ratio of $b_{2a}(\mathrm{Fe})/b_{2a}(\mathrm{Cr})$ for the trigonal distortion in fluorides is about one order of magnitude smaller than those in oxides and chlorides.

Acknowledgments

The authors offer appreciative thanks to Mr I Iwai and Mr H Mizutani for their help in the EPR experiments and analysis.

References

[1] Takeuchi H, Arakawa M, Aoki H, Yosida T and Horai K 1982 *J. Phys. Soc. Japan* **51** 3166–72
[2] Arakawa M, Ebisu H and Takeuchi H 1986 *J. Phys. Soc. Japan* **55** 2853–8
[3] Takeuchi H, Arakawa M and Ebisu H 1987 *J. Phys. Soc. Japan* **56** 4571–80
Takeuchi H, Arakawa M and Ebisu H 1990 *J. Phys. Soc. Japan* **59** 2297 (erratum)
[4] Takeuchi H, Ebisu H and Arakawa M 1991 *J. Phys. Soc. Japan* **60** 304–12
[5] Takeuchi H, Arakawa M and Ebisu H 1991 *J. Phys.: Condens. Matter* **3** 4405–20
[6] Arakawa M, Ebisu H and Takeuchi H 2002 *J. Phys.: Condens. Matter* **14** 8613–23
[7] Babel D 1967 *Struct. Bonding* **3** 1–87
[8] Arakawa M, Ebisu H and Takeuchi H 2002 EPR in the 21st century: basics and applications to material, life and earth sciences *Proc. 3rd Asia Pacific EPR/ESR Symp (Kobe, Japan, 2001)* (Amsterdam: Elsevier) pp 219–24
[9] Takeuchi H, Tanaka H, Arakawa M and Ebisu H 2005 *J. Phys.: Condens. Matter* **17** 1375–84
[10] Abragam A and Bleaney B 1970 *Electron Paramagnetic Resonance of Transition Ions* (Oxford: Clarendon)
[11] Jeck R and Krebs J J 1972 *Phys. Rev.* B **5** 1677–87
[12] Rudowicz C 1985 *J. Phys. C: Solid State Phys.* **18** 1415–30
[13] Krebs J J and Jeck R K 1972 *Phys. Rev.* B **5** 3499–505
[14] Takeuchi H, Arakawa M and Ebisu H 1987 *J. Phys. Soc. Japan* **56** 3677–82
[15] Schrama A H M 1973 *Physica* **68** 279–302
[16] Patel J L, Davies J J, Cavenett B C, Takeuchi H and Horai K 1976 *J. Phys. C: Solid State Phys.* **9** 129–38
[17] Takeuchi H, Tanaka H and Arakawa M 1993 *J. Phys.: Condens. Matter* **5** 9205–14
[18] Symmons H F and Bogle G S 1962 *Proc. Phys. Soc.* **79** 468–72
[19] Wenzel R F and Kim Y W 1965 *Phys. Rev.* A **140** 1592–8
[20] Takeuchi H and Arakawa M 1984 *J. Phys. Soc. Japan* **53** 376–80
[21] Rousseau J J, Gesland J Y, Binois M and Fayet J C 1974 *C. R. Acad. Sci.* **279** B103–5